ANNALS OF GEOPHYSICS, 56, 4, 2013, S0445; doi:10.4401/ag-6451

Special Issue: Vesuvius monitoring and knowledge

Electric effects induced by artificial seismic sources at Somma-Vesuvius volcano

Rosa Di Maio[1,*], Gianpaolo Cecere[2], Prospero De Martino[3], Ester Piegari[1]

[1] *Università di Napoli "Federico II", Dipartimento di Scienze della Terra, dell'Ambiente e delle Risorse, Naples, Italy*

[2] *Istituto Nazionale di Geofisica e Vulcanologia, Centro Nazionale Terremoti, Rome, Italy*

[3] *Istituto Nazionale di Geofisica e Vulcanologia, Sezione di Napoli, Osservatorio Vesuviano, Naples, Italy*

Article history
Received September 26, 2012; accepted January 16, 2013.
Subject classification:
Seismo-electric effects, Controlled seismic sources, Self-potential monitoring, Somma-Vesuvius volcano.

ABSTRACT

In this paper, we present a series of self-potential measurements at Somma-Vesuvius volcanic area acquired in conjunction with an active seismic tomography survey. The aim of our study is both to provide further confirmation to the occurrence of seismo-electric coupling and to identify sites suitable for self-potential signal monitoring at Somma-Vesuvius district. The data, which were collected along two perpendicular dipoles, show significant changes on the natural electric field pattern. These variations, attributable to electrokinetic processes triggered by the artificial seismic waves, were observed after explosions occurred at a distance less than 5 km from the SP dipole arrays. In particular, we found that the NW-SE component of the natural electric field was more sensible to the shots than the NE-SW one, and the major effects did not correspond to the nearest shots. Such evidences were interpreted considering the underground electrical properties as deduced by previous detailed resistivity and self-potential surveys performed in the study area.

1. Introduction

The self-potential (SP) geophysical method consists on measurement at the ground surface of anomalous potential drops at the ends of a passive line in which impolarizable electrodes are grounded. Such anomalous potentials are generated mainly by electrochemical, electrokinetic and thermoelectric sources [Sill 1983]. In particular, electrokinetic phenomena are responsible of several electrical properties of fluid-saturated porous materials. Geophysical applications of these phenomena include, for example, mapping of subsurface fluid flow, study of hydrothermal activity of geothermal areas, volcanic activity forecasting and earthquake prediction [Revil et al. 1999a].

In last four decades, many theoretical and experimental studies on physical mechanisms responsible for seismo- or volcano-electromagnetic effects have been presented [e.g., Nur 1972, Mizutani et al. 1976, Sill 1983, Varotsos and Alexopoulos 1984a,b, Johnston 1989, Fujinawa and Takahashi 1990, Di Maio and Patella 1991, Fujinawa and Takahashi 1992, Di Maio and Patella 1994, Pride 1994, Patella et al. 1997, Revil et al. 1999a,b, Uyeda et al. 2000, Garambois and Dietrich 2001, Garambois and Dietrich 2002, Garambois et al. 2002, Varotsos 2005], although most authors agree that the electrokinetic phenomenon, also called streaming potential, is the most likely source for the ultra-long period seismo-electric signals considered in this paper. Such a phenomenon is substantially caused by the electric double layer on the interface between solid and fluid in a fluid-saturated porous rock [e.g., Overbeek 1952, Keller and Frisch-knecht 1966, Mizutani et al. 1976, Morgan et al. 1989, Pride 1994]. The double layer consists of ions (mostly anions in silicate rocks) retained on the solid surface and ions of the opposite sign (cations) in the liquid phase loosely attached to the anion layer. Thus, the free liquid in the centre of the rock pore is in surplus of cations. The potential difference between the solid-liquid interface and the centre of the pore is known as the *zeta-potential*. When the liquid is forced through the porous medium, as result of a pressure gradient, the water molecules carry along with them the free positive ions in the diffusion zone of the pore. This relative movement of cations with respect to the firmly attached anions generates an electric current and hence the so-called streaming potential.

The most reliable physical model for interpreting the seismo-electric effects generated by electrokinetic phenomena is the one predicted by Onsager's theory of coupled flows [Onsager 1931], originally introduced in geophysics by Nourbehecht [1963], then comprehensively examined by Mizutani et al. [1976], Sill [1983],

Di Maio and Patella [1991], Pride [1994], Revil et al. [1999a,b], Garambois and Dietrich [2001, 2002], Garambois et al. [2002]. In brief, the quoted authors derive the general equations of particle diffusion in porous media under the action of forces related to electric potential, pressure, temperature and concentration gradients, in a general framework that includes the physical parameters characterizing the investigated media (i.e., electrical conductivity, permeability, etc). Taking into account the properties of the media where the signal propagates is crucial for modelling the self-potential anomalies associated with seismic or volcano activity. In fact, several studies [e.g., Varotsos and Lazaridou 1991, Fedorov et al. 2001] suggest that the expected magnitude of seismo-electric signals in the DC range from electrokinetic sources reach detectability threshold only for an exceptionally favorable set of crustal parameters [Uyeda et al. 2009].

It is worth noting that the detectability of seismoelectric effects is also strictly linked to the distance between the SP measurement station and the epicentre of natural or artificial seismic shots. Indeed, since the stress variation associated with the shot varies as r^{-3}, where r is the epicentral distance, seismic events of low magnitude (<4) could not be able to trigger electric field variations for epicentral distances larger than a few kilometres [Parrot et al. 1993]. The results of telluric current investigations in seismo-active areas confirm such a hypothesis [Myachkin et al. 1972, Rikitake 1987]. However, close to the epicentres, electric coseismic signals may exist, even if their intensity could be too low to be detected [Parrot et al. 1993].

In this paper, we present a series of self-potential measurements at Somma-Vesuvius volcanic area (Campania Region, Italy) performed in conjunction with artificial shots fired for active seismic experiments in the framework of the Mt. Vesuvius seismic tomography project [Gasparini et al. 1998]. By taking advance of previous detailed resistivity and self-potential surveys carried out in the Vesuvian area [Di Maio et al. 1996a,b, 1997, 1998], the study is aimed at detecting SP anomalous patterns very likely associated to the shots, in order to provide further confirmation to the occurrence of seismo-electric coupling and to identify sites suitable for SP signal monitoring at Somma-Vesuvius district.

2. Theoretical background of seismo-electric coupling

The propagation of natural or artificial seismic waves in saturated media produces electric and electromagnetic effects due to electrokinetic processes at the pore scale.

The seismoelectric coupling is frequency-dependent and its full analytical description has been derived by Pride [1994], who integrates the Biot's theory [1956] for the seismic wave propagation in a two-phase medium with Maxwell's equations. This analytical development allows numerical simulations of electrokinetic coupling phenomena in homogeneous and layered saturated media [Haartsen and Pride 1997, Garambois and Dietrich 2001, Garambois and Dietrich 2002]. In the stationary case, which is considered in this paper, the electric potential function U is given by the primary field due to active sources and the perturbation field due to induced charge distributions over conductivity discontinuity surfaces [Di Maio et al. 1998]:

$$U = \frac{1}{4\pi}\left[\int_v \frac{\nabla \cdot \mathbf{J}_{cnd}}{\sigma r} dV + \int_v \frac{\mathbf{E} \cdot \nabla\sigma}{\sigma r} dV\right], \qquad (1)$$

where J_{cnd} and E are the conduction current density and electric field vectors, respectively, σ is the electric conductivity and r is the distance from a generic observation point to any volume element dV of the conductive space. Following Sill [1983], the total current, mass and heat flows are coupled by the following equations:

$$\vec{J}_{tot} = -\gamma_{11}\nabla U - \gamma_{12}\nabla P - \gamma_{13}\nabla T, \qquad (2)$$

$$\vec{I}_{tot} = -\gamma_{21}\nabla U - \gamma_{22}\nabla P - \gamma_{23}\nabla T, \qquad (3)$$

$$\vec{q}_{tot} = -\gamma_{31}\nabla U - \gamma_{32}\nabla P - \gamma_{33}\nabla T, \qquad (4)$$

where P is the pressure, T is the temperature, γ_{11} is the electrical conductivity, γ_{12} describes the streaming potential effect [Keller and Frischknecht 1966, Mizutani et al. 1976] and γ_{13} describes the Thomson's effect [Di Maio and Patella 1991]. The first right-hand term in Equation (2) is the conduction electric current density J_{cnd}, whereas the two last terms define the convective electrical current density J_{cnv}, i.e. $J_{tot} = J_{cnd} + J_{cnv}$. In absence of external current sources, the steady state vector J_{tot} is everywhere divergence-free, which implies $\nabla \cdot J_{cnd} = -\nabla \cdot J_{cnv}$. Therefore, using Equation (2), after a few simple mathematical steps we definitively get:

$$\nabla \cdot \mathbf{J}_{cnd} = \left[\gamma_{22}\nabla\left(\frac{\gamma_{12}}{\gamma_{22}}\right)\cdot\nabla P + \gamma_{33}\nabla\left(\frac{\gamma_{13}}{\gamma_{33}}\right)\cdot\nabla T\right] - \left[\left(\frac{\gamma_{12}}{\gamma_{22}}\right)\nabla\cdot\mathbf{I}_{tot} + \left(\frac{\gamma_{13}}{\gamma_{33}}\right)\nabla\cdot\mathbf{q}_{tot}\right]. \qquad (5)$$

The first sum in square brackets shows that electrical sources develop wherever at least one of the gradients of the generalised conductivities (the γ's auto and cross-coupling coefficients) is not perpendicular to the gradient of the corresponding generalised primary potential (P or T). The second sum in square bracket shows that electrical sources generate wherever there

are impressed sources of mass and/or heat primary flows. By substituting Equation (5) in Equation (1), it is possible to derive the coupled coefficients by electric potential measurements on the ground surface.

3. Volcanological and structural setting

The Somma-Vesuvius volcanic complex is located in the southern sector of the Campania Plain, a wide peri-Tyrrhenian graben bordered by Mesozoic carbonate platforms, variously dismembered, splitted up and rotated by the Mio-Plio-Pleistocenic tectonics [Ippolito et al. 1973]. It is a strato-volcano formed by an older edifice dissected by a summit caldera, Mt. Somma, and a recent cone, Mt. Vesuvius, which grew within the caldera after the A.D. 79 Pompeii eruption [Santacroce 1987, Cioni et al. 1999].

During the last 22 ka, four plinian eruptions have occurred at Somma-Vesuvius, alternated with more frequent subplinian to strombolian and effusive episodes [Santacroce et al. 2008 and references therein]. Since the last eruption in 1944, Mt. Vesuvius is in a quiescent stage characterized by low level of seismicity and small fumarolic activity.

In the last twenty years, the knowledge of Somma-Vesuvius structural setting is strongly increased thanks to the TomoVes [Gasparini et al. 1998] and BroadVes [De Gori et al. 2001] research projects, respectively based on active seismic and teleseismic experiments. Moreover, an electro-magnetic study [Di Maio et al. 1998 and references therein], based on self-potential, resistivity tomography and magnetotelluric measurements, provided a further characterization of the shallow and deep underground structures in terms of electrical parameters. In particular, the electric surveys showed the presence of a largely extended conductive zone down to a depth of about 2 km b.g.l., closely in correspondence to the Somma caldera, including in the middle the top terminal part of the Vesuvius main plumbing system, and extending towards the Tyrrhenian sea. Conversely, the magnetotelluric soundings revealed the existence of a conductive zone ascribable to a melting trap roughly beneath the central Vesuvius apparatus at a depth of nearly 7 km and cross-section of about 2×2 km^2. These evidences well correlate with: i) the micro-earthquake activity, which shows hypocentres clustered around the vertical axis through the Vesuvius cone, with focal depths not exceeding 6 km b.s.l. [Bianco et al. 1998, Lomax et al. 2001, Zollo et al. 2002, De Natale et al. 2006], and ii) the results of an active seismic profile [Zollo et al. 1996, Auger et al. 2001], which indicates a P-to S phase conversion at a depth of about 8 km, estimated by a 2D ray-tracing model at the top of a low-velocity zone, assumed to represent a melting zone.

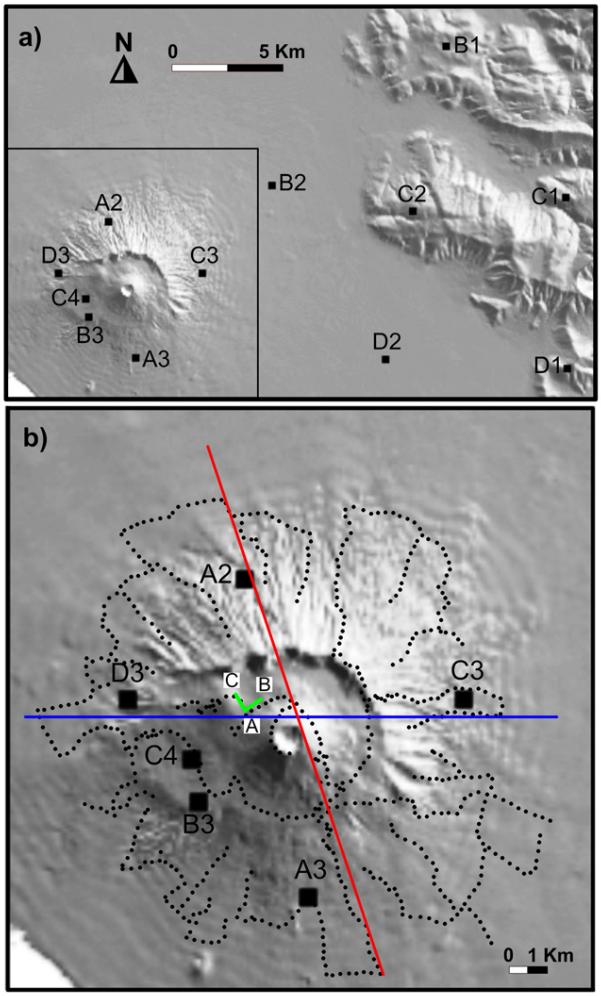

Figure 1. (a) Map showing the distribution of the shot points (black rectangles) used for the seismic tomography survey at Somma-Vesuvius (Naples, Italy). (b) Location of the AB and AC dipoles (green lines) along which the natural electric field was measured. The black points indicate the SP measurement circuits, and the red and blue lines define the resistivity tomography profiles (see text) [Di Maio et al. 1998].

4. SP data acquisition

To provide further confirmation to the occurrence of electric precursors of seismic events and to individuate sites suitable for an electroseismic signal monitoring network at Somma-Vesuvius, we monitored the SP time variations very likely induced by the TomoVes active seismic experiments performed in the volcanic complex by Gasparini et al. [1998].

The natural electric field data were acquired through two dipoles (AB and AC in Figure 1b) located on the western sector of the Vesuvius volcano at an altitude of about 850 m a.s.l. The dipole sites were selected considering the land shot distribution and the noise level of the area as well as the *selectivity* property of the measure station in capturing electric signals related to seismic phenomena. The selectivity was introduced by Varotsos and Lazaridou [1991], and is defined as the sensitivity of a station to signals from a restricted number of seismic areas while remaining insensitive to seismo-elec-

tric signals from other areas which may be closer by. A large number of empirical observations suggests that selectivity depends simultaneously on: *site characteristics* (e.g., geological inhomogeneities that cause different resistivities along different azimuths from the station); *travel path* (e.g., the physical properties, like electrical conductivity, of the main path between the station and the seismic area); *source characteristics* (e.g., the mechanism at the focus of the earthquake from which the directional properties of the emitted signal might result). The latter was obviously not taken into account in our choice of the measurement site by virtue of the artificial nature of the sources. Conversely, we focused on the first two topics by basing on the results of electro-magnetic studies [Di Maio et al. 1996a,b, 1997, 1998] previously performed in the Mt. Somma-Vesuvius volcanic district. Specifically, as the study of Varotsos and Lazaridou [1991] outlined that in a strongly inhomogeneous area, like the Vesuvius one, a geological or physical discontinuity may acts as an *amplifier* of seismoelectric signals, we positioned our dipoles in an area characterized by significant resistivity contrasts (see Section 6).

The dipoles AB and AC (see Figure 1b), perpendicular to each other, are 500 m long and consist of grounded copper-copper sulphate impolarizable electrodes. For both dipoles, the SP data were collected using different sampling rates, starting about one hour before the first shot. Table 1 reports the acquisition time intervals and the corresponding sampling rates for the days in which the SP measurements were carried out. In particular, a sampling rate of 60 s (long step) was selected to evaluate the natural polarisation trend of the site; the sampling interval of 10 s (medium step) was deputed to underline anomalous SP variations just before the shot; finally, the shorter sampling step (5 s) (short step) had to outline quick signal variations ascribable to the shot.

Figures 2-8 show the two natural electric field components, E_x and E_y, observed along the AB and AC dipoles of Figure 1, respectively. The field components were registered with long, medium and short steps for different time intervals before and after the shots. To better visualize possible SP anomalous trends caused by the shots with respect to natural background, for each figure the field components are shown for a time period of 60 minutes, of which 30 min before (black symbols) and 30 min after (red symbols) the explosions. Data are displayed with the medium time step for the intervals 10 min before the shot and 20 min after the shot, and with the long time step for the other intervals. We note that the time periods shown in Figure 3 are shorter than 60 minutes due to accidental breakdowns of the cables during the SP data acquisition.

5. SP data analysis

Looking at the figures from 2 to 8 and the location of the shot whose each one refers (see Figure 1), anomalous patterns characterizing the SP signal are only evident for data collected in conjunction with the shots in A2 (Figure 2) and B3 (Figure 3). Conversely, a very slight amplification of the natural polarisation

Day	Shots	Shot times (hh:mm:ss)	SP acquisition time intervals (hh:mm:ss)		
			Sampling rates		
			Δt = 60 s	Δt = 10 s	Δt = 5 s
1st	B1(770 kg)	19:00:00	18:21:00 - 20:00:00	18:50:00 - 19:20:00	18:55:00 - 19:15:00
2nd	D3(204 kg)	19:30:01	18:01:00 - 20:30:00	19:20:00 - 19:50:00	19:25:00-19:45:00
3rd	D2(264 kg)	19:00:00	18:01:00 - 20:00:00	18:50:00-19:20:00	18:55:00-19:15:00
	D1(800 kg)	2030:00	20:01:00 - 21:00:00	20:20:00 - 20:45:00	20:25:00 - 20:43:00
4th	C2(552 kg)	19:00:01	18:01:00 - 20:00:00	18:50:00-19:20:00	18:55:00-19:15:00
	C1(756 kg)	20:30:01	20:01:00 - 21:00:00	20:20:00 - 20:50:00	20:25:00 - 20:45:00
5th	A3 (510 kg)	19:00:00	18:01:00 - 20:00:00	18:50:00 -19:20:00	18:55:00 -19:15:00
	A2(482 kg)	20:30:00	20:01:00 - 21:00:00	20:20:00 - 20:50:00	20:25:00 - 20:45:00
6th	B2(250 kg)	19:00:01	18:01:00 - 20:00:00	18:50:00 - 19:20:00	18:55:00-19:15:00
	B3(504 kg)	20:30:01	20:01:00 - 21:00:00	20:20:00 - 20:50:00	20:25:00 - 20:45:00
7th	C3(384 kg)	19:00:01	18:01:00 - 20:00:00	18:50:00 - 19:20:00	18:55:00 - 19:15:00
	C4 (496 kg)	20:30:02	20:01:00 - 21:00:00	20:20:00 - 20:50:00	20:25:00 20:45:00

Table 1. Sampling time intervals used for the SP data acquisition along the dipoles AB and AC of Figure 1. Date, time and dynamite charge of the shots are also reported.

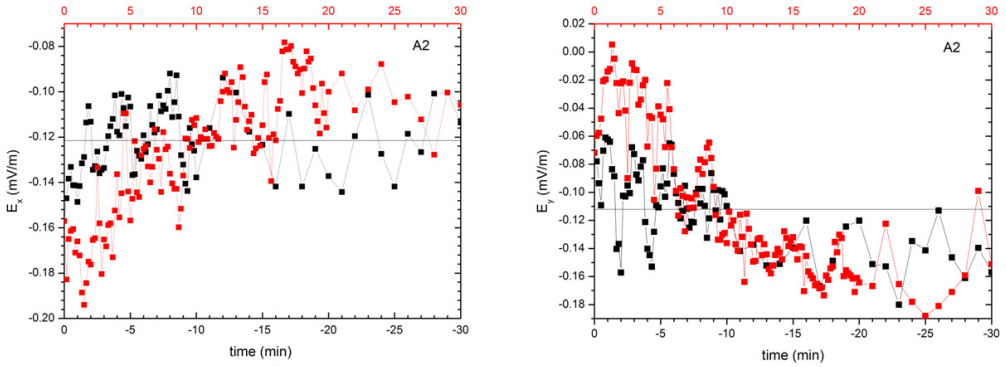

Figure 2. Natural electric field components, E_x and E_y (in mV/m), observed along the AB and AC dipoles, respectively, related to the shot in A2. Black symbols are used for data measured 30 min before the shot, while red symbols are used for data registered 30 min after the shot. The zero time of both the black and red scales corresponds to the shot time. The black continuous line represents the average value of the field component before the shot.

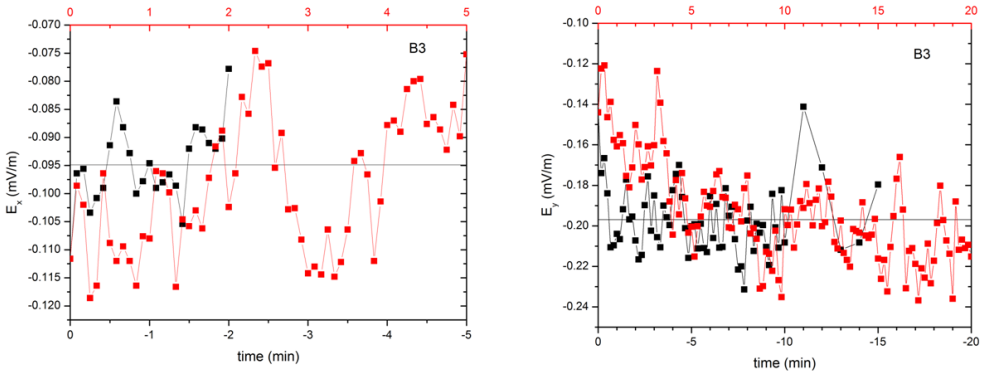

Figure 3. Natural electric field components, E_x and E_y (in mV/m), observed along the AB and AC dipoles, respectively, related to the shot in B3. Black symbols are used for data measured before the shot, while red symbols are used for data registered after the shot. The zero time of both the black and red scales corresponds to the shot time. The black continuous line represents the average value of the field component before the shot.

trend may be recognized soon afterwards the shots located in C4 e D3 (Figures 4 and 5, respectively), which are very close to the SP station sites (in any case at distances less than 5 km) and aligned along an approximately NW-SE direction.

In detail, the most significant anomalous behaviour of the natural electric field is outlined in Figure 2 for the shot point A2, which is located about 3.75 km north of the sensor A. Indeed, immediately after the shot, we observe a prominent displacement from the natural polarization trend, which is well evident for both the field components at all sampling frequencies.

A similar anomalous behaviour is shown in Figure 3, where the E_y values recorded after the shot in B3, show an increase in amplitude that lasts about 4 min. Due to lack of data acquisition along the E_x component caused, as previously mentioned, by accidental breakdown of the cable, the representation of this component is possible only for few minutes before and after the shot. In this case, clear changes are not observed, even if a small amplification of the signal seems to characterize the signal few minutes after the shot, as occurs for the behaviour of the E_x component registered after the shots in C4 and D3 (see discussion below).

Although the shot points C4 and D3 (located about 1.5 km south-west and 2.5 km west, respectively, of the electrode A) are closer than B3 to the SP station sites, no clear anomalous trends can be observed in the collected SP time series (see Figure 4a,b and Figure 5a,b). The lack of clear evidences could be ascribed to the significant dispersion of the natural background as well as to the physical properties of the volumes involved by the seismic ray paths. However, to try to highlight possible seismo-electric effects, we have calculated the Fast Fourier Transform (FFT) of the electric field components registered 5 min before and 5 min after the shots C4 and D3. For example, Figures 4c and 5c show the time series of the E_x component acquired with the short time step (5s), and Figures 4d and 5d report the corresponding FFT. As shown in these last figures, the component at zero frequency of the time series observed 5 min after the shots (i.e., the mean value of the signal) is larger than the one observed before the shots. Moreover, as pointed out by the arrows in Figure 4d, an increase is observed in the amplitude of the signal oscillations after the shot C4 with periods $T_1 \approx 1$ min

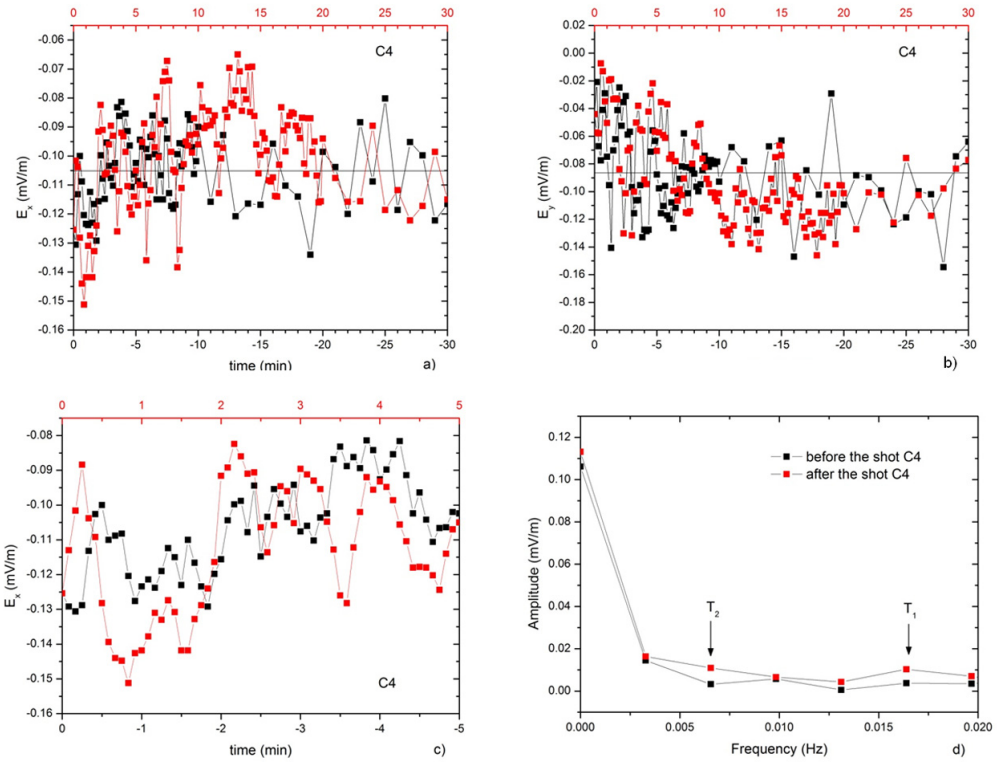

Figure 4. Natural electric field components, E_x and E_y (in mV/m), observed along the AB and AC dipoles and related to the shot in C4, are shown respectively in (a) and (b). (c) Time series of the E_x component registered with the short step (5s) 5 min before and 5 min after the shot. Black symbols are used for data measured before the shot, while red symbols are used for data registered after the shot. The zero time of both the black and red scales corresponds to the shot time. The black continuous line represents the average value of the field component before the shot. (d) FFT of the signal shown in (c).

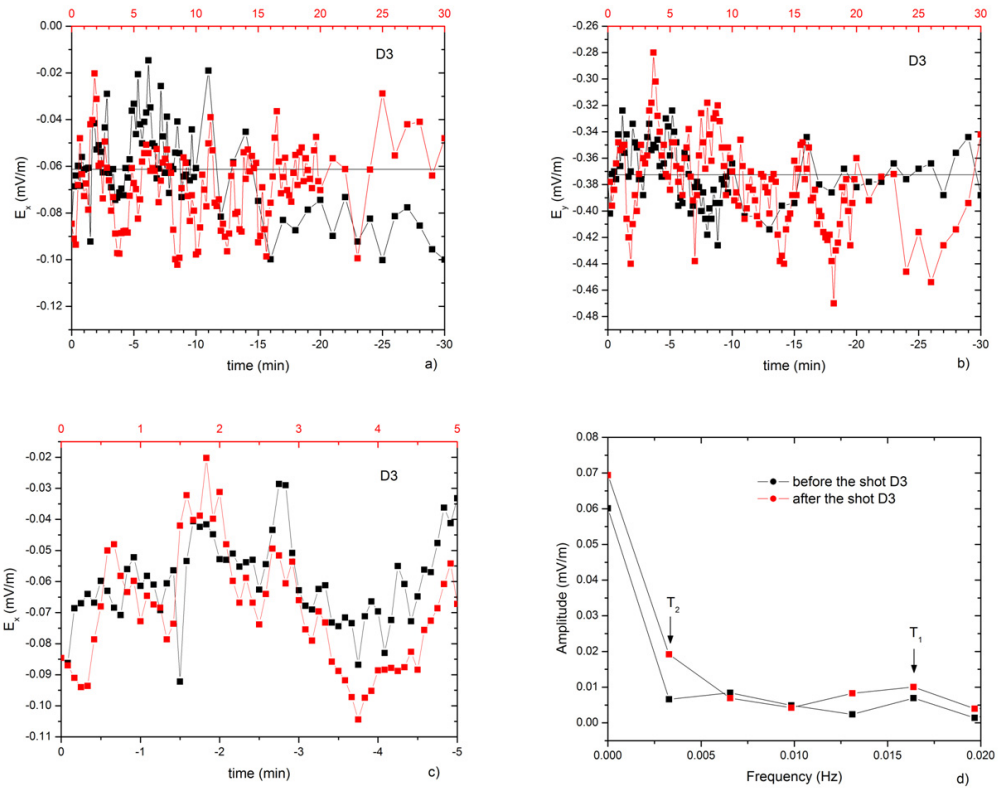

Figure 5. Natural electric field components, E_x and E_y (in mV/m), observed along the AB and AC dipoles and related to the shot in D3, are shown respectively in (a) and (b). (c) Time series of the E_x component registered with the short step (5s) 5 min before and 5 min after the shot. Black symbols are used for data measured before the shot, while red symbols are used for data registered after the shot. The zero time of both the black and red scales corresponds to the shot time. The black continuous line represents the average value of the field component before the shot. (d) FFT of the signal shown in (c).

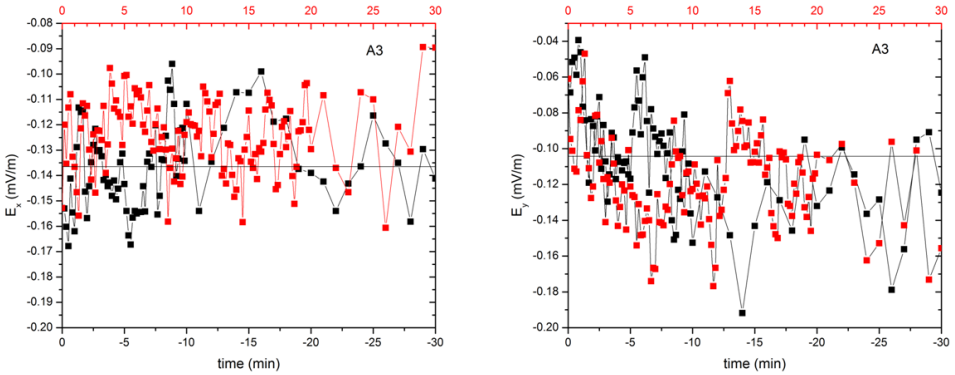

Figure 6. Natural electric field components, E_x and E_y (in mV/m), observed along the AB and AC dipoles, respectively, related to the shot in A3. Black symbols are used for data measured 30 min before the shot, while red symbols are used for data registered 30 min after the shot. The zero time of both the black and red scales corresponds to the shot time. The black continuous line represents the average value of the field component before the shot.

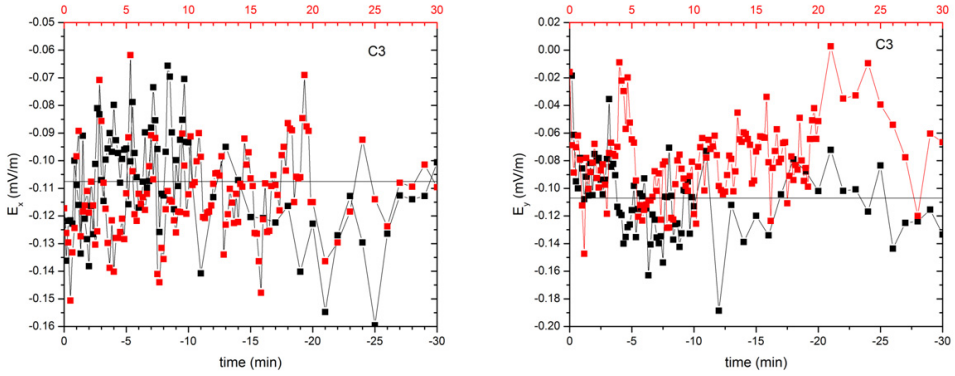

Figure 7. Natural electric field components, E_x and E_y (in mV/m), observed along the AB and AC dipoles, respectively, related to the shot in C3. Black symbols are used for data measured 30 min before the shot, while red symbols are used for data registered 30 min after the shot. The zero time of both the black and red scales corresponds to the shot time. The black continuous line represents the average value of the field component before the shot.

and $T_2 \approx 2.5$ min. A similar increase in the amplitude of the FFT is found for the E_x component after the shot in D3 with periods $T_1 \approx 1$ min and $T_2 \approx 5$ min (see Figure 5d). Such features could be indicative of possible seismo-electric effects of small scale, due to the physical properties of the involved volumes and the site-specific characteristics of the shot points (see Figure 10).

As concerns the shot points A3 and C3, no appreciable changes are observed in the field components recorded after the shots, as shown in Figures 6 and 7, respectively. We notice that A3 is nearly symmetric to the shot point A2 with respect to the SP station sites, and, thus, the lack of a significative anomalous electric effect, as the one registered after the shot in A2, can be attributed to different physical characteristics of the volume affected by the seismic ray-paths related to the shot A3 (see also Figure 10).

Furthermore, no evident variations are observed in the field components recorded after the shots in B2, B1, C1, C2, D1 and D2 that are far from SP station sites much more than 5 km. For example, we show in Figure 8 the time series related to the shots in B2 and D1.

Finally, if we look at the Figure 9, which displays the electric polarization vectors related to the SP registrations, it is quite clearly that the shots in B3 and A2 are very likely responsible for the changes in the polarisation vector amplitudes (see Figure 9e,f), and possibly the same occurs (but to a lesser extent) for the shots D3 and C4 (see Figure 9b,g).

6. SP data interpretation

The SP data analysis discussed in the previous section has outlined that only the seismic explosions located to a distance not greater than 5 km from our SP measuring dipoles have induced anomalous variations on the natural electric field of the selected area. Such a small distance, ascribable to the low magnitude of the seismic events caused by the explosions (see the explosive amounts in Table 1), seems compatible with the distances to which electric signals are observed [Parrot et al. 1993].

However, many anomalous features observed on the natural electric field pattern, which we have tentatively ascribed to electric effects induced by the artificial

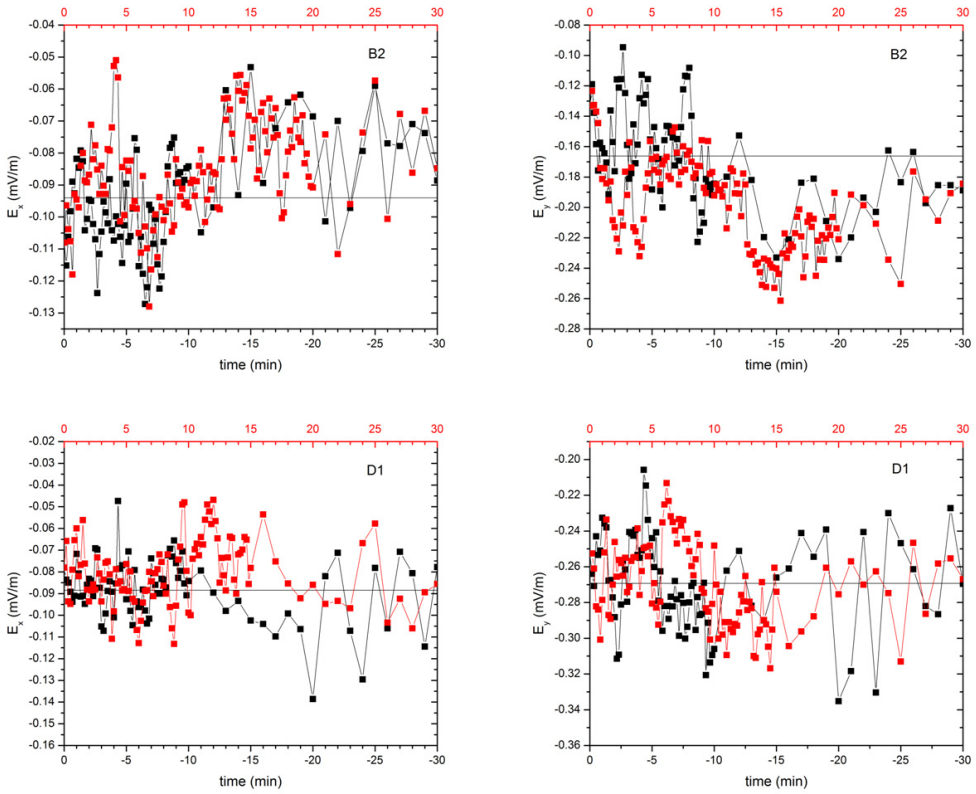

Figure 8. Natural electric field components, E_x and E_y (in mV/m), observed along the AB and AC dipoles, respectively, related to the shots in B2 and D1. Black symbols are used for data measured 30 min before the shot, while red symbols are used for data registered after the shot. The zero time of both the black and red scales corresponds to the shot time. The black continuous line represents the average value of the field component before the shot.

seismic sources, do not appear of immediate interpretation. In particular, i) almost all the data sets shown in the Figures 2-8 outline an E_y component more sensible to the seismic signals than the E_x component; ii) the anomaly observed after the shot A2 is much more prominent than those observed after the shots located very close to the measuring arrays (i.e., D3, C4 and B3); iii) the explosion in A3, sited symmetrically to the shot point A2 with respect our station site, has not caused significative effects on the pattern of the natural electric field components.

These apparently *anomalous* features could be justified if we refer to the selectivity property of the measuring site [Varotsos and Lazaridou 1991], i.e. its sensitivity to capture electric signals induced by seismic phenomena coming from areas not necessarily located near the measuring station. As the selectivity effect mainly depends on the geological and physical characteristics of the measurement site as well as on the physical properties of the seismic wave travel path, we interpret the SP anomalies observed immediately after the shots by taking into account the electric outline of the Mt. Somma-Vesuvius structural setting as deduced by our previous geoelectrical studies in the Vesuvian area [Di Maio et al. 1996a,b, 1997, 1998] that, for reader convenience, are shown below. Specifically, we will refer to results of a SP survey performed in an area of about 170 km^2 and of two resistivity tomographies carried out along two nearly perpendicular profiles (see Figure 1b).

Figure 10 shows the SP anomaly map and the 3D tomographic inversion of the SP data (i.e. the underground electric charge distributions very likely responsible of the observed anomalies), while the Figure 11 illustrates the 2D tomographic inversion of the apparent resistivity data acquired along the approximately N-S and W-E profiles of Figure 1b. For further details about measuring system, survey technique and data processing, the reader is referred to the above mentioned papers. Looking at the Figures 10 and 11, strong inhomogeneties of both geological and physical characteristics of the investigated buried volumes are well evident. In particular, the main negative and positive charge accumulation areas, extending from the ground surface down to a depth of about 2 km b.s.l., well describe the Mt. Somma caldera rim and the central Vesuvius chimney. Such structural lineaments strictly correlate with the roughly horizontal alternation of resistive and conductive bodies shown in Figure 11. Indeed, the highly resistive deep bodies well define the Somma caldera rims, while the inner conductive body closely corresponds to the summit of the Vesuvius central edifice. Following Di Maio et al. [1998], the northern highly resistive body may be ascribed to a slowly cooled compact magmatic dike, while the low resistiv-

ities that characterise the Vesuvius central plumbing system may be correlated to the presence of highly conductive fluids and/or pores occluded by hydrothermal alteration particles. Finally, the southern discontinuous resistive block may be ascribed to a thick sequence composed of ancient submarine lavas, locally intercalated with clayey and muddy beds, and to the underlying carbonate basement, according to the stratigraphy of the Trecase-1 geothermal well [Balducci et al. 1985].

At the light of the above-described electrical characterization of the surveyed volcanic complex, we interpret the anomalous electric signals observed right after the artificial shots as follows: the greater sensitivity to electroseismic signals of the E_y component with respect to the E_x component of the natural electric field could be justified by the presence of the northern highly resistive structure (i.e., the supposed lava dyke), nearly located beneath the AC measuring dipole, and of the resistivity low in the central Vesuvius edifice (see Figure 11). In fact, as experienced by Varotsos and Lazaridou [1991], the contact between two media characterised by different resistvity values induces on the electric field component perpendicular to the contact a discontinuity which depends on the ratio of the resistivities of the two media. Therefore, appreciable SP variations are mainly observed on the E_y component, since the AC dipole extends along a structural discontinuity characterized by high-resistivity contrast, while the AB dipole is located in the central part of the volcanic apparatus distinguished by weak contrasts.

In the area under investigation, this *local* characteristic of the selectivity effect certainly superimposes onto the *large-scale* characteristics due to the above mentioned physical and structural inhomogeneities. Such a consideration may well explain the lack of significant seismoelectric signals induced by shot points located very near to our measuring dipoles. Indeed, considering the artificial seismic shot distribution of Figure 1, is reasonable to assume that the seismic waves generated by the shots in D3 and C4 have crossed the strongly fractured and altered central plumbing system outlined by the geoelectrical survey. Such a high conductivity structure may have caused a significant loss of the seismic wave energy not allowing the triggering of electrokinetic processes responsible of seismoelectric effects (see Section 1). The shot B3, even if is not far

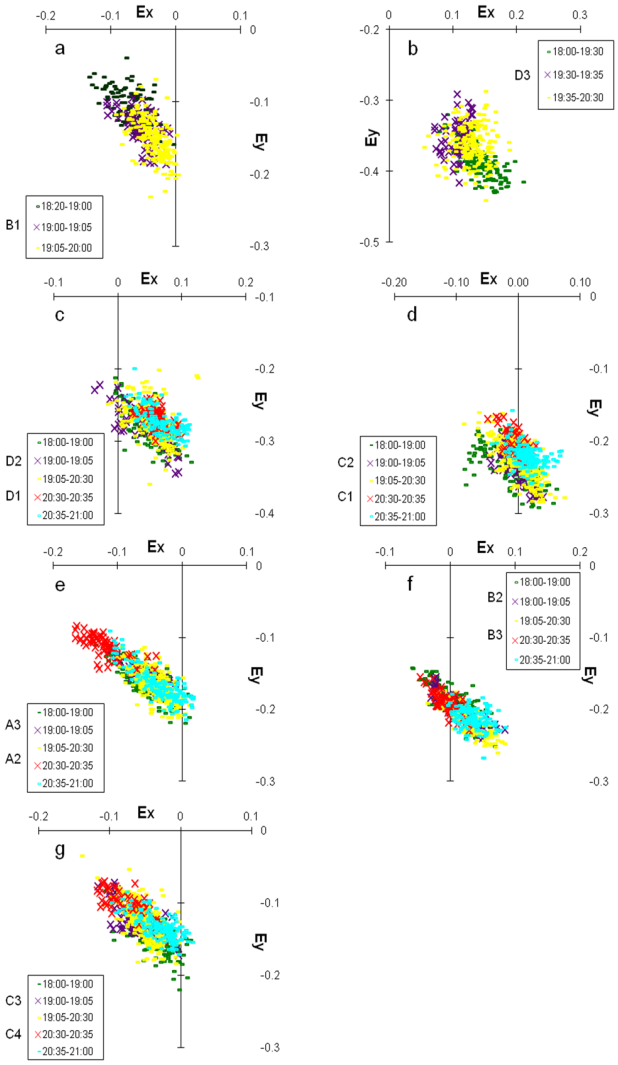

Figure 9. Electric polarization vectors related to the field components, E_x and E_y (in mV/m), observed before and after the shots in Figure 1.

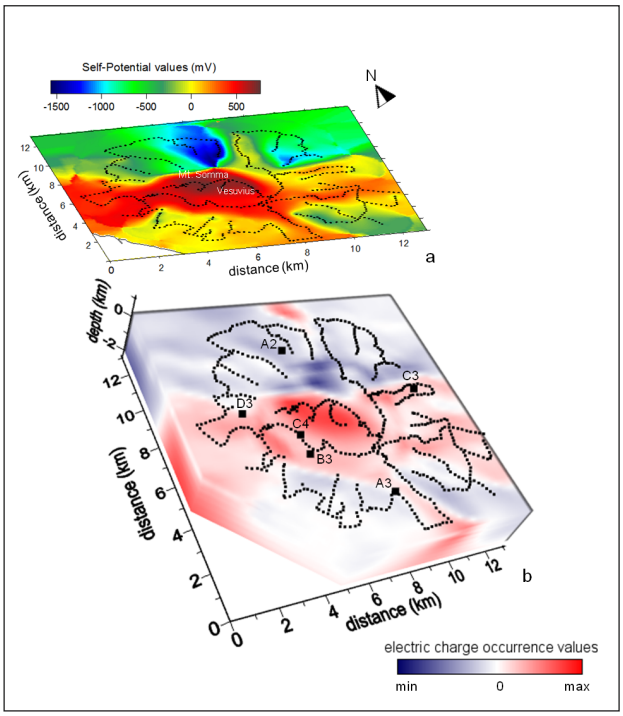

Figure 10. Results of the self-potential survey performed in the Mt. Somma-Vesuvius area along the circuits shown in Figure 1b. (a) SP anomaly map, redrawn after Di Maio et al. [1998]. (b) Volumetric view of the 3D inversion of the SP data shown in (a). The volume data are reported with a clipping plane that allows to visualize a section parallel to the SP survey area of Figure 1b at a depth of about 150 m above sea level. The black rectangles indicate the location of the shot points.

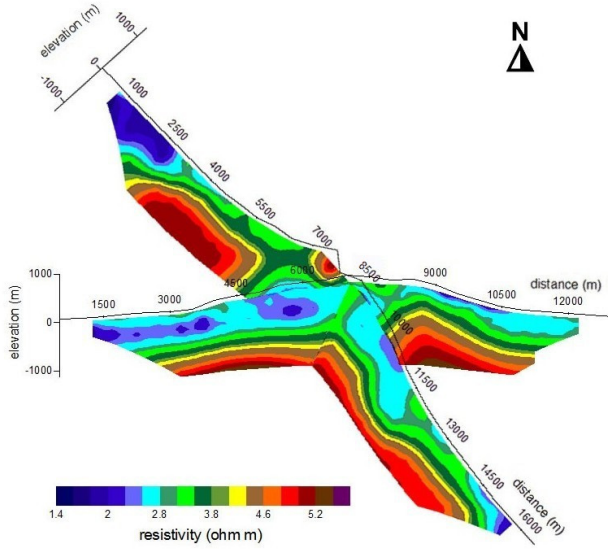

Figure 11. Intersection of the 2D resistivity tomographies carried out along the approximately N-S and W-E profiles of Figure 1b.

from D3 and C4, is closer to a charge accumulation zone extending in the NW direction and this could explain the evidence of a more evident anomalous trend in the E_y field component. On the contrary, the shot points in C3 and A3, respectively sited in the eastern and southern sectors of the volcanic apparatus, are located in regions of charge deficiency, which may explain a significant reduction of seismoelectric signals.

Finally, we notice that the time span of the SP anomalies observed after the shots is comparable with that observed for the seismoelectric precursor signals. Such evidences bring us to hypothesise that electrofiltration processes or, equivalently, electrokinetic effects (see Section 1) could justify the natural electric field variations induced by the artificial seismic sources at Mt. Somma-Vesuvius. The presence in some sectors of the study-area of a large amount of fluids, which are most probably highly mineralized, constitutes an effective support to our hypotheses.

7. Conclusions

A large number of both theoretical and experimental studies has outlined anomalous electric signals preceding earthquakes. Thus, variations on the natural electric field pattern present as good candidates both for monitoring fracturing mechanisms precursor of earthquakes and for testing numerical modelling of magma propagation based on stress-induced fracturing mechanisms [Eichelberger 1995, Scandone et al. 2007, Piegari et al. 2008, Piegari et al. 2011].

The results of this study, although referred to artificial seismic sources and, therefore, related to the occurrence of co-seismic electric signals, provide further evidence that their origin is linked to electrokinetic processes that generate in fluid-saturated porous rocks. In particular, our study outlined a higher sensibility of the vertical electric field component with respect to the horizontal component. Furthermore, it was observed that the most striking effects were not induced by the proximity to the shots, but rather by the presence of both deep largely extended high resistivity bodies and contrasts in the physical properties of the buried structures. The interpretation of these apparent anomalous features, which was based on the electric characteristics of the volumes affected by the seismic tomography survey, seems to confirm that the occurrence of seismoelectric signals depends both on site geostructural characteristics and on seismic wave travel path, i.e. the selectivity property of the station site [Varotsos and Lazaridou 1991].

Concluding, the knowledge of the electric setting of seismically active areas is fundamental to planning an electroseismic signal monitoring network, as signals emitted from certain seismic areas cannot be felt by some stations in the network, independently of the earthquake magnitude and epicentral distances, in virtue of the geostructural and physical properties of the volumes involved in the related seismic phenomena.

Acknowledgements. We wish to thank two anonymous Reviewers for their valuable comments that help us to improve our manuscript.

References

Auger, E., P. Gasparini, J. Virieux and A. Zollo (2001). Seismic evidence of an extended magmatic sill under Mt. Vesuvius, Science, 294, 1510-1512.

Balducci, S., M. Vaselli and G. Verdiani (1985). Exploration well in the 'Ottaviano' permit, Italy; 'Trecase 1', In: A.S. Straub and P. Ungemach (eds.), European Geothermal Update, Proc. 3rd Int. Seminar on the results of EC Geothermal Energy Research, Reidel, Dordrecht.

Bianco, F., M. Castellano, G. Milano, G. Ventura and G. Vilardo (1998). The Somma-Vesuvius stress field induced by regional tectonic: evidences by seismological and mesostructural data, J. Volcanol. Geoth. Res., 82, 199-218.

Biot, M.A. (1956). The theory of propagation of elastic waves in a fluid-saturated porous solid. I. Low-frequency range. II. Higher frequency range, J. Acoust. Soc. Am., 28, 168-191.

Cioni, R., R. Santacroce and A. Sbrana (1999). Pyroclastic deposits as a guide for reconstructingthe multistage evolution of the Somma-Vesuvius caldera, Bull. Volcanol., 53, 287-300.

De Gori, P., G.B. Cimini, C. Chiarabba, G. De Natale, C. Troise and A. Deschamps (2001). Teleseismic tomography of the Campanian volcanic area and sur-

rounding Apenninic belt, J. Volcanol. Geoth. Res., 109, 52-75.

De Natale, G., C. Troise, F. Pingue, G. Mastrolorenzo and L. Pappalardo (2006). The Somma-Vesuvius volcano (Southern Italy): Structure, dynamics and hazard evaluation, Earth-Science Reviews, 74 (1/2), 73-111.

Di Maio, R., and D. Patella (1991). Basic theory of electrokinetic effects associated with earthquakes, Boll. Geofis. Teor. Appl., 33 (130/131), 145-154.

Di Maio, R., and D. Patella (1994). Self-potential anomaly generation in volcanic areas. The Mt. Etna case-history, Acta Vulcanologica, 4, 119-124.

Di Maio, R., G. Cecere, P. De Martino and P. Vietri (1996a). Tomografie elettriche al Mt. Somma-Vesuvio, VI Workshop di GeoElettroMagnetismo (Santa Margherita Ligure, Italy, September 18-20, 1996).

Di Maio, R., V. Di Sevo, S. Giammetti, D. Patella, S. Piscitelli and C. Silenziario (1996b). Self-potential anomalies in some Italian volcanic areas, Annali di Geofisica, 39 (1), 179-188.

Di Maio, R., P. Mauriello, D. Patella, Z. Petrillo, S. Piscitelli, A. Siniscalchi and M. Veneruso (1997). Self-potential, geoelectric and magnetotelluric studies in Italian active volcanic areas, Annali di Geofisica, 40 (2), 519-537.

Di Maio, R., P. Mauriello, D. Patella, Z. Petrillo, S. Piscitelli and A. Siniscalchi (1998). Electric and electromagnetic outline of the Mount Somma-Vesuvius structural setting, J. Volcanol. Geoth. Res, 82 (1/4), 219-238.

Eichelberger, J.C. (1995). Silicic volcanism: ascent of viscous magmas from crustal reservoirs, Annu. Rev. Earth Planet. Sci., 23, 41-63.

Fedorov, E., V. Pilipenko and S. Uyeda (2001). Electric and magnetic fields generated by electrokinetic processes in a conductive crust, Phys. Chem. Earth, C26, 793-799.

Fujinawa, Y., and K. Takahashi (1990). Emission of electromagnetic radiation preceding the Ito seismic swarm of 1989, Nature, 347, 376-378.

Fujinawa, Y., and K. Takahashi (1992). A study of anomalous underground electric field associated with a volcanic eruption, Geophys. Res. Lett., 19 (1), 9-12.

Garambois, S., and M. Dietrich (2001). Seismo-electric wave conversions in porous media: Field measurements and transfer function analysis, Geophysics, 66, 1417-1430.

Garambois, S., and M. Dietrich (2002). Full-waveform numerical simulations of seismo-electromagnetic wave conversions in fluid-saturated stratified porous media, J. Geophys. Res., 107 (B7); doi:10.1029/2001 JB000316.

Garambois, S., P. Seneshal and H. Perrod (2002). On the use of combined geophysical methods to assess water content and water conductivity of near-surface, Journal of Hydrology, 259, 32-48.

Gasparini, P., and TomoVes Working Group (1998). Looking inside Mt. Vesuvius, EOS, 79, 229-232.

Haartsen, M., and S. Pride (1997). Electroseismic waves from point sources in layered media, J. Geophys. Res., 102 (B11), 24745-24769; doi: 10.1029/97JB02936.

Ippolito, F., F. Ortolani and M. Russo (1973). Struttura marginale tirrenica dell'Appennino Campano: reinterpretazione di dati di antiche ricerche di idrocarburi, Mem. Soc. Geol. It., 12, 227-250.

Johnston, M.J.S. (1989). Review of magnetic and electric field effects near active faults and volcanoes in the U.S.A., Phys. Earth Planet. Inter., 57, 47-63.

Keller, G.V., and F.C. Frischknecht (1966). Electrical Methods in Geophysical Prospecting, Pergamon, Oxford, 526 pp.

Lomax, A., A. Zollo, P. Capuano and J. Virieux (2001). Precise, absolute earthquake location under Somma-Vesuvius volcano using a new 3D velocity model, Geophys. J. Int., 146 (2), 313-331.

Mizutani, H., T. Ishido, T. Yokokura and S. Ohnishi (1976). Electrokinetic phenomena associated with earthquakes, Geophys. Res. Lett., 3, 365-368.

Morgan, F.D., E.R.Williams and T.R. Madden (1989). Streaming potential properties of Westerly Granite with applications, J. Geophys. Res., 94, 12449-12461.

Myachkin, V.I., G.A. Sobolev, N.A. Dolbilkina, V.N. Morozov and V.B. Preobrazensky (1972). The study of variations in geophysical fields near focal zones of Kamchatka, Tectonophysics, 14 (3/4), 287-293.

Nourbehecht, B. (1963). Irreversible thermodynamic effects in inhomogenous media and their application in certain geoelectric problems, Ph. D. thesis. M.I.T., Cambridge.

Nur, A. (1972). Dilatancy, pore fluids and premonitory variations of ts/tp travel times, Bull. Seismol. Soc. Am., 62, 1217-1222.

Onsager, L. (1931). Reciprocal relations in irreversible processes. I., Phys. Rev., 37, 405-426.

Overbeek, J.Th.G. (1952). Electrochemistry of the double layer, In: H.R. Kruyt (ed.), Colloid Science: Irreversible Systems, vol. 1, New York, Elsevier, 115-193.

Parrot, M., J. Achache, J.J. Berthelier, E. Blanc, A. Deschamps, F. Lefeuvre, M. Menvielle, J.L. Plantet, P. Tarits and J.P. Villain (1993). High-frequency seismo-electromagnetic effects, Phys. Earth Planet. Inter., 77, 65-83.

Patella, D., A. Tramacere and R. Di Maio (1997). Modelling earth current precursors in earthquake prediction, Annali di Geofisica, 40 (2), 495-517.

Piegari, E., V. Cataudella, R. Di Maio, L. Milano, M. Nicodemi and R. Scandone (2008). A model of volcanic magma transport by fracturing stress mechanisms, Geophys. Res. Lett., 35, L06308(4); doi:10.1029/2007GL032710.

Piegari, E., R. Di Maio, R. Scandone and L. Milano (2011). A cellular automaton model for the rise of magma: degassing and styles of volcanic eruptions, J. Volcanol. Geoth. Res., 202, 22-28; doi:10.1016/j.jvolgeores.2011.01.007.

Pride, S. (1994). Governing equations for the coupled electromagnetics and acoustics of porous media, Physical Review B, 50 (21), 15678-15696.

Revil, A., P.A. Pezard and P.W.J. Glover (1999a). Streaming potential in porous media. 1. Theory of the zeta potential, J. Geophys. Res., 104 (B9), 20021-20031.

Revil, A., H. Schwaeger, L.M. Cathles and P. Manhardt (1999b). Streaming potential in porous media. 2. Theory and application to geothermal systems, J. Geophys. Res., 104 (B9), 20033-20048.

Rikitake, T. (1987). Magnetic and electric signals precursory to earthquakes: an analysis of Japanese data, J. Geomagn. Geoelectr., 39, 47-61.

Santacroce, R., ed. (1987). Somma-Vesuvius, Quaderni de "La Ricerca Scientifica", CNR, 114 (Progetto finalizzato Geodinamica, Monografie finali, 8), 251 pp.

Santacroce, R., R. Cioni, P. Marianelli, A. Sbrana, R. Sulpizio, G. Zanchetta, D. J. Donahue and J.L. Joron (2008). Age and whole rock-glass compositions of proximal pyroclastics from the major explosive eruptions of Somma-Vesuvius: A review as a tool for distal tephrostratigraphy, J. Volcanol. Geoth. Res., 177 (1), 1-18.

Scandone, R., K. Cashman and S.D. Malone (2007). Magma supply, magma ascent and the style of volcanic eruptions, Earth Planet. Sci. Lett., 253, 513-529; doi:10.1016/j.epsl.2006.11.016.

Sill, W.R. (1983). Self-potential modeling from primary flows, Geophysics, 48 (1), 76-86; doi:10.1190/1.1441409.

Uyeda, S., T. Nagao, Y. Orihara, T. Yamaguchi and I. Takahashi (2000). Geolectric potential changes: Possible precursors to earthquakes in Japan, Proc. Natl. Acad. Sci. U.S.A., 97, 4561-4566.

Uyeda, S., T. Nagao and M. Kamogawa (2009). Short-term earthquake prediction: Current status of seismo-electromagnetics, Tectonophysics, 470, 205-213.

Varotsos, P., and K. Alexopoulos (1984a). Physical properties of the variations of the electric field of the earth preceding eartquakes, I, Tectonophysics, 110, 73-98.

Varotsos, P., and K. Alexopoulos (1984b). Physical properties of the variations of the electric field of the earth preceding earthquakes, II. Determination of epicenter and magnitude, Tectonophysics, 110, 99-125.

Varotsos, P., and M. Lazaridou (1991). Latest aspects of eartquake prediction in Greece based on seismic electric signals, Tectonophysics, 188, 321-347.

Varotsos, P.A. (2005). The Physics of Seismic Electric Signals, Tokyo, TerraPub.

Zollo, A., P. Gasparini, J. Virieux, H. Le Meur, G. De Natale, G. Biella, E. Boschi, P. Capuano, R. De Franco, P. Dell'Aversana, R. De Matteis, I. Guerra, G. Iannaccone, L. Mirabile and G. Vilardo (1996). Seismic evidence for a low-velocity zone in the upper crust beneath Mount Vesuvius, Science, 274, 592-594.

Zollo, A., L. D'Auria, R. De Matteis, A. Herrero, J. Virieux and P. Gasparini (2002). Bayesian estimation of 2-D P velocity models from active seismic arrival time data: imaging of the shallow structure of Mt. Vesuvius (Southern Italy), Geophys. J. Int. 151, 566-582.

*Corresponding author: Rosa Di Maio,
Università di Napoli "Federico II", Dipartimento di Scienze della Terra, dell'Ambiente e delle Risorse, Naples, Italy;
email: rosa.dimaio@unina.it.